Direct evidence for inelastic neutron "acceleration" by ^{177}Lu^m

O. Roig,[1,*] V. Méot,[1] B. Rossé,[1] G. Bélier,[1] J.-M. Daugas,[1] A. Letourneau,[2] A. Menelle,[3,4] and P. Morel[1]

[1]*CEA, DAM, DIF, F-91297 Arpajon, France*

[2]*CEA, IRFU, Service de Physique Nucléaire, Centre de Saclay, F-91191 Gif-sur-Yvette, France*

[3]*CEA, DSM, LLB, F-91191 Gif-sur-Yvette, France*

[4]*CNRS, INP UMR12, F-91191 Gif-sur-Yvette, France*

The inelastic neutron acceleration cross section on the long-lived metastable state of ^{177}Lu has been measured using a direct method. High-energy neutrons have been detected using a specially designed setup placed on a cold neutron beam extracted from the ORPHEE reactor in Saclay. The 146 ± 19 b inelastic neutron acceleration cross section in the ORPHEE cold neutron flux confirms the high cross section for this process on the ^{177}Lu^m isomer. The deviation from the 258 ± 58 b previously published obtained for a Maxwellian neutron flux at a 323 K temperature could be explained by the presence of a low energy resonance. Resonance parameters are deduced and discussed.

I. INTRODUCTION

Inelastic neutron acceleration (INNA), also called superelastic neutron scattering, occurs during the collision of a neutron with an excited nucleus. In this reaction, the nucleus transfers part of its excitation energy to the scattered neutron. Predicted since 1959 [1], this process was observed 20 years later on two isomeric nuclei, ^{152}Eu^m [2] and ^{180}Hf^m [3]. The effect of this neutron-induced de-excitation is known in nuclear astrophysics to take place in the *s*-process nucleosynthesis [4–7]. Thanks to the usually high cross section of thermal neutron interaction, such a process could be used to induce a fast de-excitation of an isomer. The 160-day $J^\pi = 23/2^-$ isomer in ^{177}Lu ($Ex = 970$ keV) and the 31-year $J^\pi = 16^+$ ^{178}Hf^{m2} [8] are good candidates to directly observe the inelastic neutron acceleration reaction. The 258 ± 58 b high value of the thermal INNA reaction cross section for ^{177}Lu^m has been indirectly deduced from burn-up [9] and capture cross sections [10]. Such an analysis has recently been achieved for INNA by the ^{178}Hf^{m2} with an estimated cross section of 168 ± 33 b [8]. In the case of ^{177}Lu^m, the radiative capture cross section has been extracted under two reasonable hypothesis: (i) the ^{177}Lu$^m(n,\gamma)^{178}$Lu^m cross section corresponds to the total radiative capture cross section; (ii) the existence of an unknown long-lived isomer which could trap a part of the γ decay is very unlikely. The goal of this work is (i) to confirm the existence of the INNA process in the interaction of neutrons and ^{177}Lu^m, and (ii) to confirm the high cross-section value of the INNA process.

In this we report on the INNA cross section on ^{177}Lu^m obtained by a direct measurement of emitted neutrons. The high-energy neutrons coming from the reaction between the long-lived isomer of ^{177}Lu and cold neutrons were counted using a neutron multidetector array at the ORPHEE reactor facility. The presence of a low energy resonance and its resonance parameters were deduced from a comparison of this

INNA cross section in a cold neutron flux to the previously published value obtained in a thermal neutron flux. We discuss the relevance of these latter results.

II. EXPERIMENTAL METHOD

A. The ^{177}Lu^m target

The production of an easy-to-handle target of ^{177}Lu^m has been undertaken several times [11,12] at the Laue Langevin Institute (ILL) in Grenoble (France). For this measurement, a natural lutetium foil (25 μm thickness) of mass (10.24 ± 0.01) mg was irradiated at the high flux reactor (HFR) at the ILL to produce ^{177}Lu^m by the radiative capture reaction ^{176}Lu(n,γ). The V4 port located close to the core of the HFR was used to benefit from the maximum neutron flux, around 1.5×10^{15} n cm^{-2} s^{-1}. The natural Lu foil was put inside an aluminum capsule and was irradiated during 6 days. After a 150-day cooling time it was put inside a thin pure aluminum envelope (20 μm thick). The number of $(1.03 \pm 0.05) \times 10^{14}$ isomers was accurately measured by γ spectroscopy right before the experiment at the ORPHEE reactor facility. The activity of this radioactive target was 13.22 MBq. A similar nonirradiated natural lutetium foil from the same natural lutetium sample used for the isomer target was used as a blank target.

B. The ORPHEE facility

The isomeric target produced at the HFR was moved to the ORPHEE facility in Saclay to perform the experiment. The ORPHEE facility managed by the Léon Brillouin laboratory (LLB) is built around a research nuclear reactor. The 14-MW reactor ORPHEE is made of a 56 dm^3 highly enriched ^{235}U core, surrounded by a heavy water reflector tank to get a good thermal neutron flux of 3×10^{14} n cm^{-2} s^{-1}. Several cold neutron beams are extracted along neutron guides emerging from the reactor building. For this experiment, we used the G3.2 experimental area located about 40 m away from the reactor core. The neutron guides are composed of multilayered
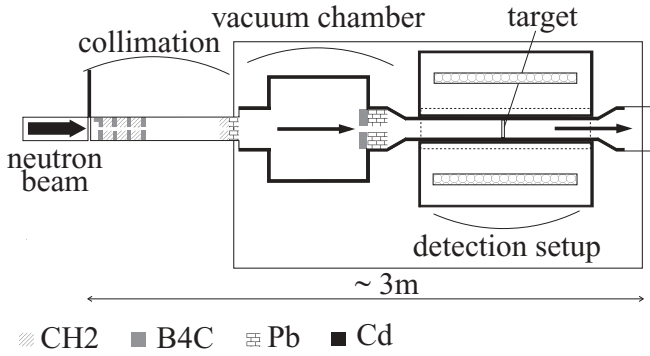
*olivier.roig@cea.fr

FIG. 1. Setup scheme.

FIG. 2. The neutron detector for the ORPHEE experiment.

nickel-titanium mirrors and are slightly curved in order to suppress the fast neutrons and γ ray background from the core. The internal section of the G3.2 neutron guide is 25×50 mm^2, giving a neutron flux of 1.5×10^9 n cm^{-2} s^{-1} for a mean energy of 4.5 meV and an angular spreading of $0.4°$. In order to decrease the background and to increase the detection efficiency, the neutron beam is collimated to a diameter of 2 cm. The collimator shown in Fig. 1 is made of a sandwich of 0.5-cm-thick boron carbide (B$_4$C) neutron absorber, followed by a 1-cm-thick polyethylene (CH$_2$) layer and a 2-cm-thick lead (Pb) γ attenuator placed 1.8 m upstream from the target. A second collimator, made of a 1-cm-thick B$_4$C and a 5-cm-thick Pb layer, is placed 25 cm from the target in order to eliminate neutrons scattered on the first collimator.

C. The neutron detector

The main difficulty in this experiment is to overcome the low signal-to-background ratio. Two background sources have to be considered. The first one is due to scattered cold neutrons. To limit this counting rate a dedicated chamber has been built to work under vacuum. The second one is due to photons from neutron captures and the γ activity of the target itself. The 10-bar pure ^{3}He proportional counter from Saint-Gobain Company was chosen because of its low sensitivity to γ rays. Its outer diameter is 2.54 cm and its active length is 25 cm. Despite the high photon flux, the neutron detection is unaffected because the deposited energy is small and associated with a very low efficiency. Moreover, the neutron detection is obtained via the exothermic reaction: $n + {}^3\text{He} \rightarrow {}^3\text{H} + p$, whose Q value is 764 keV. Tests with a very intense ^{60}Co source showed that the thermal neutron peak located at 764 keV was not affected by photon fluxes up to 10^7 ph/s on the detector. To detect high-energy neutrons, a slowing down neutron counter was used [13]. The neutron array consists of a cylindrical polyethylene moderator combined with 12 proportional ^{3}He counters placed inside the moderator. Fast neutrons produced in the target scatter many times in the moderator and quickly slow down by elastic scattering reactions to the thermal neutron energy. Under these conditions, the ^{3}He detectors have a large efficiency to detect these thermal neutrons. The inner part of the vacuum chamber is shielded by a 2-mm-thick cadmium layer to suppress the neutrons scattered by the target. An outside 1-mm-thick
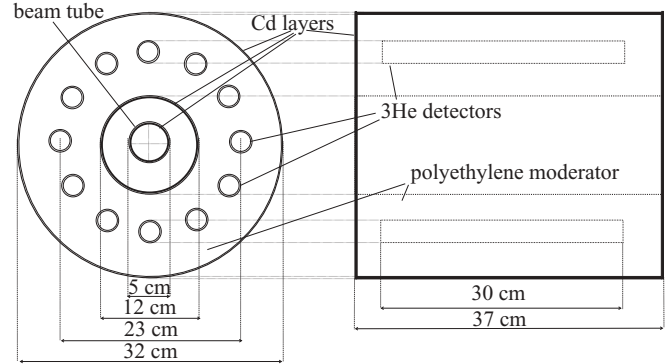
layer of cadmium covers the whole cylindrical polyethylene moderator in order to stop all thermal neutrons coming from the background or cold neutrons scattered by the collimator. The cadmium layer lets high-energy neutrons come into the polyethylene cylinder where they lose their energy. Figure 2 shows front and side views of the neutron array, including dimensions.

The neutron array was simulated using the Monte Carlo code MCNP [14] to get the thermal neutron total efficiency. Emitted neutrons from the INNA process on the isomeric target should strictly have energies up to the isomeric level energy, 970 keV. Looking at the selection rules and the transmission coefficients given in Ref. [9], neutron energies should likely be comprised between 100 and 500 keV. The efficiency of the neutron array shown in Fig. 3 was obtained using the MCNP code. Error bars in Fig. 3 come from statistical uncertainties. The efficiency in the range of expected neutron energies is more or less flat with a mean efficiency of 19.8% (see Fig. 3). A very similar response was obtained using the Monte Carlo code GEANT4 [15]. However, our simulation does not take into account the electronic threshold and the wall effect in the ^{3}He tubes. The correction factor was obtained by measuring and simulating the neutron activity of a known ^{252}Cf source positioned in the target holder. The ^{252}Cf spontaneous fission neutron spectrum was simulated using MCNP code through a
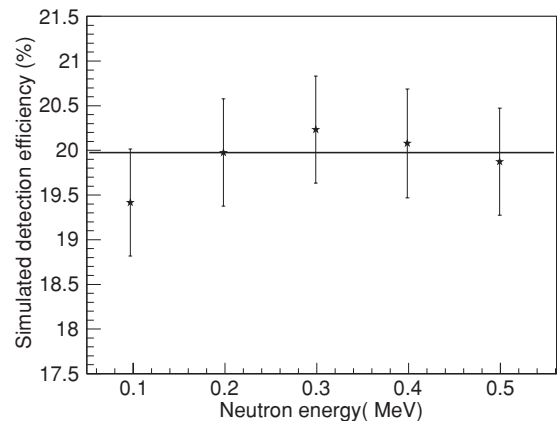

FIG. 3. Detection efficiency of the neutron array obtained from MCNP simulations. Black line represents the mean value of the detection efficiency.

Watt spectrum with parameters described in [14]. The activity of the ^{252}Cf source at the time of the experiment was (1479 ± 66) n s^{-1} in 4π. The source was 18 years old, allowing its use without corrections cited in [16]. The corrected detection efficiency is then $(18.4 \pm 0.9)\%$.

D. Neutron flux determination

The neutron flux must be determined at the target position. We used the ^{175}Lu present in the radioactive target itself to get the neutron flux value at the target position. As the reaction ^{175}Lu$(n,\gamma)^{176}$Lu^m also takes place during the experiment in the radioactive target, the activation of the ^{176}Lu^m isomer produced by these reactions can be directly used to get the neutron flux by knowing the precise amount of ^{175}Lu. The sample mass was determined by weighing. From this quantity, the amount of ^{175}Lu present in the isomeric target could be determined with accuracy by knowing the initial ^{175}Lu quantity, the neutron flux in the V4 port at the ILL high-flux reactor, and the cross sections of the burn-up of ^{175}Lu. The burn-up correction is 1.75%. The obtained amount of ^{175}Lu, $N_{^{175}\text{Lu}}$, is (9.80 ± 0.01) mg.

The activation of the ^{176}Lu^m [$T_{1/2} = 3.664$ h, $\lambda_{^{176}\text{Lu}^m} = (5.25 \pm 0.03) \times 10^{-5}$] isomer was measured just after the irradiation at the ORPHEE G3.2 point. A low-energy photon spectrometer (LEPS) was used to measure the 88.361-keV γ ray from the β decay of ^{176}Lu^m. A γ self-absorption correction was applied to this measurement. Figure 4 shows the γ spectrum of the isomeric target before and after the experiment. The 88.361-keV γ line clearly appears and its integral $N_{88\,\text{keV}}$ is extracted. The reaction rate per nucleus, R, is

$$R = \frac{N_{88\,\text{keV}}}{N_{^{175}\text{Lu}}} \frac{\lambda_{^{176}\text{Lu}^m} \times e^{\lambda_{^{176}\text{Lu}^m} t_{cl}}}{(1 - e^{-\lambda_{^{176}\text{Lu}^m} \cdot t_{ct}})(1 - e^{-\lambda_{^{176}\text{Lu}^m} t_{irr}}) I_{88\,\text{keV}} \times \epsilon}, \quad (1)$$

where $I_{88\,\text{keV}}$ is the intensity of the 88.361-keV γ line, and t_{irr}, t_{cl}, and t_{ct} are the time of irradiation, cooling, and counting, respectively.

The γ detection efficiency of the LEPS detector located at (55.1 ± 0.5) cm was carefully obtained using standard
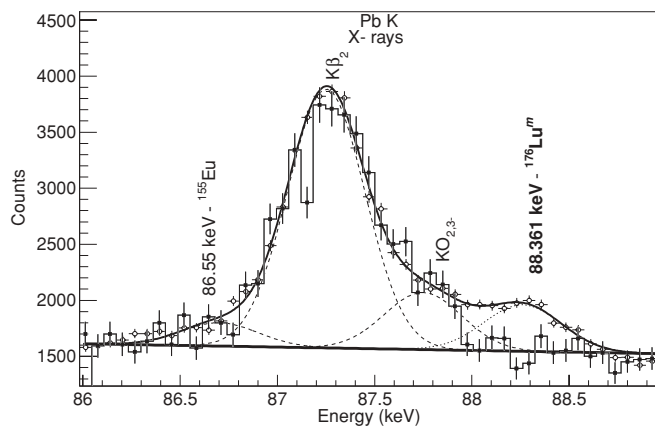
FIG. 4. γ-energy spectrum of the isomeric target showing the activation of the ^{176}Lu^m. Dark squares show data from the isomeric target before irradiation. Open circles represent data from the isomeric target after irradiation.

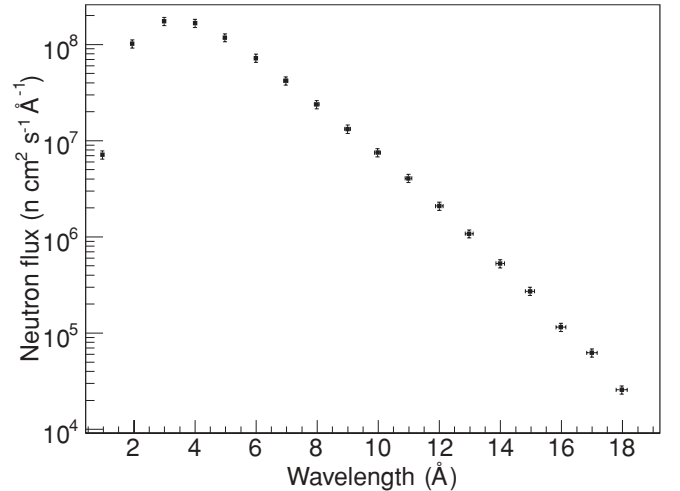FIG. 5. Neutron flux measured at the ORPHEE G3.2 facility [18].

radioactive sources (^{133}Ba, ^{152}Eu, and ^{241}Am), and MCNP [14], GEANT4 [15] simulations. This method provides a precise efficiency curve [17]. The efficiency ϵ of the setup to detect the 88.361-keV γ ray was determined at $(2.3 \pm 0.1) \times 10^{-3}$ %.

To extract the flux we need to know the value of the ^{175}Lu$(n,\gamma)^{176}$Lu^m cross section in the ORPHEE G3.2 cold neutron flux. The reaction rate R can be written as

$$R = \int_0^\infty \phi(\lambda)\,\sigma(\lambda)\,d\lambda = \phi_b \int_0^\infty S(\lambda)\,\sigma(\lambda)\,d\lambda, \quad (2)$$

where ϕ is the neutron flux (n cm^{-2} s^{-1} eV^{-1}), ϕ_b is the total neutron flux (n cm^{-2} s^{-1}), λ the neutron wavelength, $S(\lambda)$ the previously determined ORPHEE G3.2 neutron spectrum [18], and σ the capture cross section of the beam monitor. Considering a $1/v$ law for the cross section in the energy range of the neutron flux, the integration gives

$$R = \phi_b \frac{\sigma_0}{\lambda_0} \int_0^\infty S(\lambda)\,\lambda\,d\lambda = 2.487 \times \phi_b\,\sigma_0 \quad (3)$$

where σ_0 is the ^{175}Lu$(n,\gamma)^{176}$Lu^m cross section at $E_0 = 0.025$ eV ($\lambda_0 = 1.805$ Å), equal to (16.7 ± 0.4) b [19]. The integral value, 2.487, was obtained by a calculation method based on the trapezoidal rule using the sequence of points shown in Fig. 5. In the ORPHEE G3.2 cold neutron flux, the ^{175}Lu$(n,\gamma)^{176}$Lu^m cross section is then (41.5 ± 1.0) b.

Finally, using this value and the ^{176}Lu^m activation measurement, we obtain a neutron flux of $(1.71 \pm 0.16) \times 10^8$ n cm^{-2} s^{-1} on the target.

III. MEASUREMENTS AND DATA ANALYSIS

The measurement of the INNA process consists of counting the thermal neutrons detected in the neutron array. The countings were performed for different conditions related to the target and the neutron beam. Afterward, a set of fixed conditions is called a configuration and a summary of all configurations is presented in Table I. Integrals of thermal neutron peaks at 764 keV were extracted for these various configurations. The counting rates, reported in Table I, were obtained from these integrals. They were corrected for the

TABLE I. Counting rates for various configurations. Beam means that the beam is inside the cave where the neutron detector and the isomeric target are located. Beam stop is related to a block made in B_4C which lays just in front of the isomeric target, letting the neutron beam come inside the experimental cave. Statistical and systematic uncertainties are reported in the form ($\pm$statistical$\pm$systematic).

Target	Beam	Beam stop	Counting rate (cps)
$^{177}Lu^m$	On	Out	$(4.07 \pm 0.01 \pm 0.08)$
Natural Lu 14 mg	On	Out	$(2.86 \pm 0.01 \pm 0.08)$
Natural Lu 12.2 mg	On	Out	$(2.87 \pm 0.01 \pm 0.08)$
Natural Lu 6.8 mg	On	Out	$(2.79 \pm 0.01 \pm 0.08)$
No	On	Out	$(2.565 \pm 0.005 \pm 0.08)$
Al envelope alone	On	Out	$(2.637 \pm 0.003 \pm 0.08)$
$^{177}Lu^m$	On	In	$(2.690 \pm 0.010 \pm 0.08)$
$^{177}Lu^m$	Off	Out	$(1.139 \pm 0.003 \pm 0.08)$
No	Off	Out	$(1.21 \pm 0.04 \pm 0.08)$

slight flux variation using the reactor thermal power log file. The counting rate with the neutron beam impinging the Lu radioactive target is $(4.07 \pm 0.01 \pm 0.08)$ cps. The error bar includes statistical and systematic components in the form ($\pm$stat.$\pm$syst.). For estimation of the systematic uncertainty, we performed various measurements under similar conditions.

All components of the background were detailed and measured: high activity of the target, background arising from the collimation of the beam, neutron scattering on the target and neutrons from the environment (presence of the reactor, natural radioactivity). In order to determine the contribution of each of these backgrounds, we performed different measurements. The true count of thermal neutrons corresponding to the high energy neutrons is obtained by subtracting all the backgrounds from the full configuration.

By analyzing of all these configurations, we find the following:

(i) The intrinsic background without beam and isomeric target is $1.21 \pm 0.04 \pm 0.08$ cps.

(ii) When the isomeric target is put inside the reaction chamber with no beam, the counting rate is $(1.139 \pm 0.003 \pm 0.08)$ cps. No effect coming from the radioactivity of the isomeric target has been observed.

(iii) The background coming from the beam inside the chamber without the isomeric target is $2.565 \pm 0.005 \pm 0.08$ cps. This measurement shows that a large part of the background comes from the presence of the beam inside the chamber (mainly from collimators upstream from the target position).

(iv) We performed a measurement by stopping the neutron beam in a B_4C block a few centimeters in front of the isomeric target. The counting rate is then $2.690 \pm 0.010 \pm 0.08$ cps. This measurement confirms that the target radioactivity has no influence.

(v) The contribution of the neutrons scattered on the target was controlled by means of natural lutetium targets surrounded by an aluminum envelope as was the

isomeric target. For 6.8 mg, 12.2 mg, and 14 mg, the corresponding counting rates are, respectively, $(2.79 \pm 0.01 \pm 0.08)$ cps, $(2.87 \pm 0.01 \pm 0.08)$ cps, $(2.86 \pm 0.01 \pm 0.08)$ cps.

(vi) The influence of the aluminum envelope is determined using an empty aluminum envelope. The counting is then $(2.637 \pm 0.003 \pm 0.08)$ cps.

From all these measurements, the systematic error on the counting rate is estimated to be 0.08 cps. It comes mainly from the uncertainty in replacing the sample at the exact target position into the reaction chamber. Table I sums up all these counting rates.

Figure 6 shows the response function of the neutron array for these different configurations. The true counting rate of thermal neutrons corresponding to the high-energy neutrons is obtained by subtracting all backgrounds from the full configuration. The result obtained is $(1.20 \pm 0.01 \pm 0.08)$ neutrons/s.

The observed signal, (1.20 ± 0.08) neutrons/s, could be explained neither by the target radioactivity nor the cold neutron scattered by the target. The information gathered in these measurements is summarized by attributing the signal to the INNA process. From the knowledge of the neutron flux, the detection efficiency, and the number of ^{177}Lu isomers, the INNA cross section is (363 ± 48) b.

IV. DISCUSSION

This measurement confirms the existence and the high intensity of the superelastic scattering process in the interaction between slow neutrons and the high-spin isomer $^{177}Lu^m$, ($J^\pi = 23/2^-$). Table II shows INNA cross sections for both direct (this work) and indirect [9] measurements. In order to
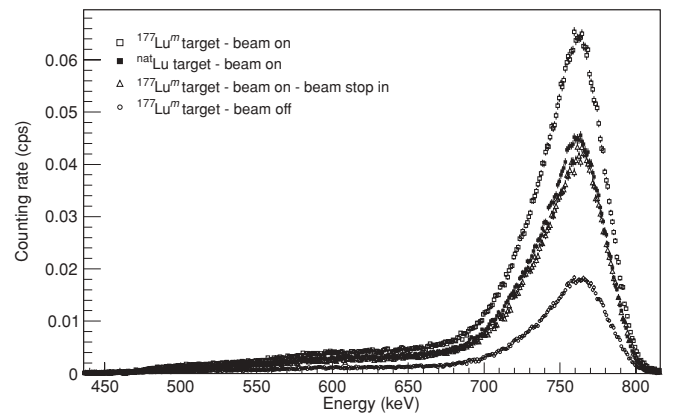

FIG. 6. Signals from the ^{3}He detectors for the different configurations studied. Energy axis is related to the deposited energy due mainly to the neutron interaction in ^{3}He detector. Open-circle symbol corresponds to a configuration with the isomeric target and without beam at the target position. Open-triangle symbol is related to configuration with the isomeric target at the target position, with beam stopped by a B_4C block just before the target. Black square symbol concerns the 14-mg natural Lu foil at the target position. Open-square symbol corresponds to the full configuration, $^{177}Lu^m$ target, and beam at the target position. Only statistical errors (cps) are reported here.

TABLE II. INNA cross sections for both direct (this work) and indirect [9] measurements. See Sec. IV for a detailed discussion about these results.

Flux	Cross section (b)
ORPHEE G3.2 cold neutron flux	363 ± 48 (this work)
Maxwellian flux at $T = 323$ K	258 ± 58 [9]

compare the value obtained from this work to the INNA cross section published at $T = 323$ K, we have to estimate a value of cross section in a similar flux. This cross-section estimation depends on the presence of resonances at low neutron energy.

If there is no resonance at low neutron energy, the INNA cross section varies as $1/v$. We can divide the measured value, (363 ± 48) b, by the factor 2.487 as explained above in Eq. (3). Although the obtained value, (146 ± 19) b, is different from the previously published value, (258 ± 58) b [10], the discrepancy lies inside about a 2-σ difference, so there is a non-negligible probability that the two results are consistent.

If a neutron resonance is present at low energy, the $1/v$ law cannot be applied to the INNA cross section. To illustrate this effect, the integrated cross section has been calculated over a Maxwellian neutron energy distribution at $T = 323$ K and over the ORPHEE G3.2 neutron energy distribution. The cross section is then described by the Breit-Wigner formula with one isolated resonance. The resonance energy, E_R, the radiative width, Γ_γ, and the neutron width, $\Gamma_{neutron}$, are adjusted on the Maxwellian averaged radiative capture cross section. This set of obtained parameters, given in Table III, is not unique but it allows the relevance of the presence of a low energy resonance to be tested. The superelastic neutron width, Γ_{SE}, is fixed at 70% of the radiative width as given by measurements at thermal neutron energy [9,10]. With the resonance parameters given in Table III, the calculated Maxwellian-averaged INNA capture cross section, at $T = 323$ K, is 260 b compared to (258 ± 58) b, and the calculated ORPHEE G3.2 INNA cross section is 374 b compared to (363 ± 48) b. Figure 7 shows the INNA cross section, the Maxwellian neutron energy spectrum ($T = 323$ K), and the ORPHEE G3.2 neutron spectrum. The presence of a low energy resonance could explain the apparent disagreement between the two measurements.

To check whether these resonance parameters are realistic, we performed calculations of their expected average value. Indeed, for such neutron energies the parameters are unpredictable and only statistical distributions around an estimated value could be calculated.

TABLE III. Resonance parameters.

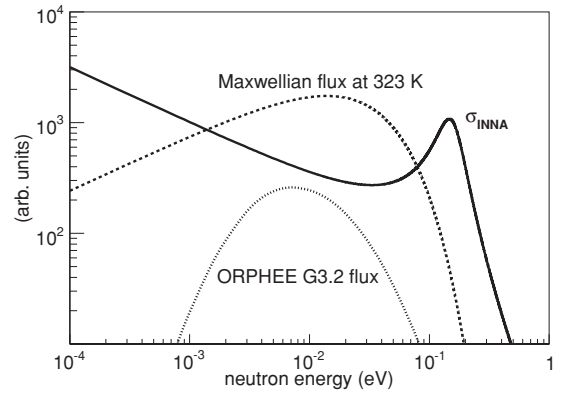|	
E_R	0.15 eV
Γ_γ	50 meV
$\Gamma_{neutron}$	1.8×10^{-2} meV
Γ_{SE}	35 meV

FIG. 7. INNA calculated cross section for $n + {}^{177}\text{Lu}^m$ reaction. Black curve is the Breit-Wigner cross section for an isolated resonance with the parameters given in Table III. Dotted curve is the Maxwellian neutron flux at $T = 323$ K and the dashed curve is the ORPHEE G3.2 cold neutron flux.

At low energy the neutron resonance spins are 11^- and 12^-. The averaged level spacing, D_0, is the inverse of the level density, given here by the Gilbert-Cameron formula [20]. The $\langle \Gamma_\gamma \rangle$ is determined from the radiative transmission coefficient, T_γ, as

$$\langle \Gamma_\gamma \rangle = k \frac{T_\gamma D_0}{2\pi}. \qquad (4)$$

Calculation of the radiative transmission coefficient is based on a γ-ray strength function given by Kopecky and Uhl [21]. The normalization factor k is adjusted on known resonance radiative widths of ${}^{175}\text{Lu}$ and ${}^{176}\text{Lu}$.

Using a deformed optical potential [22], we calculated the S-wave neutron strength function, $S_0 = 1.98 \times 10^{-4}$. The neutron width is then estimated from S_0 by the relation

$$\langle \Gamma_n \rangle = \sqrt{E_R} D_0 S_0. \qquad (5)$$

Using the same optical potential, the superelastic width is determined from the neutron transmission coefficients which are calculated for various orbital momenta carried by the emitted neutron [9].

Table IV summarizes the calculated parameters. Compared to the expected average values, the resonance parameters given in Table III are in reasonable agreement. Finally, we have pointed out how such a resonance described by

TABLE IV. Expected average value of resonance parameters. The two values for the Γ_γ come from the choice of the normalization factor obtained either from ${}^{175}\text{Lu}$ or ${}^{176}\text{Lu}$.

D_0	1.4 eV
$\langle \Gamma_\gamma \rangle$	$55 - 95$ meV
$\langle \Gamma_{neutron} \rangle$	10^{-2} meV
$\langle \Gamma_{SE} \rangle$	6 meV

these resonance parameters can be used to understand the disagreement between the cross sections measured in the thermal and cold neutron fluxes. This explanation seems more likely than reconsidering the determination of the radiative capture cross section.

The high value of the INNA cross section at very low neutron energy, supported by this direct measurement, shows that this process is very efficient to de-excite a *K*-isomer. The magnitude of the ratio between the superelastic neutron and the radiative widths, 0.7, means that the overlap between the compound nucleus and nuclear states of the residual nucleus plays a major role. The observation of several low-energy neutron resonances built on the ^{177}Lu^m isomer may shed light on nuclear structure at high excitation energy.

V. CONCLUSION

The inelastic neutron acceleration cross section on the long-lived isomer state of ^{177}Lu^m has been measured in a cold neutron beam. This result, although different, confirms the high value of our previous indirect measurement [9]. The observed difference between the two values is in favor of the presence of a low energy resonance. This work shows that the interaction of very-low-energy neutrons with the ^{177}Lu^m is the most efficient mechanism to induce an isomer de-excitation.

ACKNOWLEDGMENTS

[1] Yu. V. Petrov, Zh. Eksp. Teor. Fiz **37**, 1170 (1959) [Sov. Phys. JETP **10**, 833 (1960)].

[2] I. A. Kondurov, E. M. Korotkikh, and Yu. V. Petrov, JETP Lett. **31**, 232 (1980).

[3] I. A. Kondurov, E. M. Korotkikh, Yu. V. Petrov, and G. I. Shuljak, Phys. Lett. B **106**, 383 (1981).

[4] Y. V. Petrov and A. I. Shlyakhter, Astrophys. J. **278**, 385 (1984).

[5] F. Käppeler, J. Phys. G **14**, s297 (1988).

[6] F. Käppeler, H. Beer, and K. Wisshak, Rep. Prog. Phys. **52**, 945 (1989).

[7] N. Patronis, S. Dababneh, P. A. Assimakopoulos, R. Gallino, M. Heil, F. Käppeler, D. Karamanis, P. E. Koehler, A. Mengoni, and R. Plag, Phys. Rev. C **69**, 025803 (2004).

[8] S. A. Karamian and J. J. Carroll, Phys. Rev. C **83**, 024604 (2011).

[9] O. Roig *et al.*, Phys. Rev. C **74**, 054604 (2006).

[10] G. Bélier *et al.*, Phys. Rev. C **73**, 014603 (2006).

[11] L. Maunoury *et al.*, Nucl. Phys. A **701**, 286c (2002).

[12] O. Roig *et al.*, Nucl. Instrum. Methods Phys. Res. A **521**, 5 (2004).

[13] D. Dore, P. M. Dighe, E. Berthoumieux, J. M. Laborie, X. Ledoux, V. Macary, S. Panebianco, and D. Ridikas, in *4th International Workshop on Nuclear Fission and Fission-Product Spectroscopy*, edited by A. Chatillon, H. Faust, G. Fioni, D. Goutte, and H. Goutte, Vol. 1175 of *AIP Conference Proceedings*, pp. 277–284 (2009).

[14] J. F. Briesmeister, LA-13709-M, Los Alamos National Laboratory Report (2000), [http://lib-www.lanl.gov/cgi-bin/getfile?la-13709.htm].

[15] S. Agostinelli *et al.*, Nucl. Instrum. Methods Phys. Res. A **506**, 250 (2003).

[16] N. J. Roberts and L. N. Jones, Radiat. Prot. Dosim. **126**, 83 (2007).

[17] K. Jackman and S. Biegalski, J. Radiol. Nucl. Chem. **279**, 355 (2009).

[18] A. Menelle (private communication).

[19] S. F. Mughabghab, *Atlas of Neutron Resonances* (Elsevier Science, 2007).

[20] A. Gilbert and A. G. W. Cameron, Can. J. Phys. **43**, 1446 (2002).

[21] J. Kopecky and M. Uhl, Phys. Rev. C **41**, 1941 (1990).

[22] P. Romain and J.-P. Delaroche, *Proceedings of a NEA Specialist Meeting on the Nucleon-Nucleus Optical Model up to 200 MeV*, edited by OECD-NEA, Vol. 528 (Bruyères-le-Châtel, France, 1996), p. 167.